

TIME REVERSAL FOCUSING OF ELASTIC WAVES IN PLATES FOR EDUCATIONAL  
DEMONSTRATION PURPOSES

Christopher Heaton

Physics 492R Capstone Report submitted to the faculty of  
Brigham Young University  
in partial fulfillment of the requirements for the degree of

Bachelor of Science

Brian E. Anderson, Advisor

Department of Physics and Astronomy

Brigham Young University

August 2016

Copyright © 2016 Christopher Heaton

All Rights Reserved

## ABSTRACT

# TIME REVERSAL FOCUSING OF ELASTIC WAVES IN PLATES FOR EDUCATIONAL DEMOSTRATION PURPOSES

Christopher Heaton

Department of Physics and Astronomy

Bachelor of Science

The purpose of this research is to develop a visual demonstration of time reversal focusing of vibrations in a thin plate. Various plate materials are tested to provide optimal conditions for time reversal focusing. Specifically, the reverberation time in each plate and the vibration coupling efficiency from a shaker to the plate are quantified to illustrate why a given plate provides the best spatially confined focus as well as the highest focal amplitude possible. A single vibration speaker and a scanning laser Doppler vibrometer (SLDV) are used to provide the time reversal focusing. Salt is sprinkled onto the plate surface to allow visualization of the high amplitude, spatially localized time reversal focus; the salt is thrown upward only at the focal position. Spatial mapping of the vibration focusing on the plate using the SLDV is correlated to the visual salt jumping demonstration. The time reversal focusing is also used to knock over an object when the

object is placed at the focal position; some discussion of optimal objects to use for this demonstration are given.

## ACKNOWLEDGMENTS

This research was made possible through the help and expertise of Dr. Anderson. I would like thank the department of Physics and Astronomy for the use of their laboratory and equipment. Special thanks to Sarah Young who assisted with the experimental and measurement processes. I would also like to thank my wife for her encouragement through the time of this research.

# **Contents**

<b>Table of Contents</b> .....	6
<b>List of Figures</b> .....	7
<b>List of Tables</b> .....	8
<b>I. Introduction</b> .....	10
<b>II. Experiment Setup</b> .....	11
<b>III. Results</b> .....	19
<b>IV. Demonstration</b> .....	21
<b>V. Conclusion</b> .....	27
<b>Bibliography</b> .....	29

## List of Figures

1	Diagram and photograph of the experiment setup .....	13
2	Sample signals from a time reversal experiment.....	14
3	Deconvolution time reversal (TR) signals obtained on the glass plate.....	18
4	Spatial maps of the energy at the time of peak time reversal focusing .....	20
5	Evolution of the time reversal focusing over time .....	22
6	Photograph of salt jump visualization .....	24
7	Photographs of time reversal focusing being used to knock over objects.....	26

## **List of Tables**

1	List of the plate materials used in this study, their densities, and their sizes .....	12
2	Table of $RT60$ , $\eta$ , $f_P$ , $A_P$ , $\xi_T$ ,and $\xi_S$ .....	21



## I. Introduction

Time Reversal (TR) is a method that allows waves to be focused at an arbitrarily selected location away from a source point.<sup>1,2</sup> TR focusing has been used in several applications. These applications include underwater acoustics, biomedical ultrasound imaging and therapy, nondestructive evaluation, and seismology. TR, originally termed matched signal processing, was first employed in fluid media to provide underwater acoustic communication between ships,<sup>3</sup> and it continues to be explored and refined for this application.<sup>4,5</sup> TR has been used to focus waves in elastic media to locate and characterize cracks in mechanical parts,<sup>6,7</sup> communicate signals along pipes,<sup>8</sup> and in seismology to locate the epicenter of earthquakes,<sup>9</sup> and geophysical tremor.<sup>10</sup> In addition, time reversal has medical applications. Through the use of time reversal, a kidney stone in the body can be located and destroyed during lithotripsy treatment.<sup>11-12</sup>

One method of achieving time reversal focusing, sometimes termed reciprocal time reversal, is to obtain an impulse response between locations A and B in a sample or medium. Location A represents the location of the source. Location B represents the location of the sensor, and is where the energy focusing is desired. The impulse response is a recording of all the waves paths traversed from A to B over the time period of the recording. This impulse response is then reversed in time and broadcast from A to B (other TR methods broadcast the reversed impulse response from B to create a focus at A). The waves then retrace their original paths and are timed such that they constructively interfere at B.

The purpose of this paper is to describe an inexpensive demonstration of TR focusing of vibrational waves in thin plates. At the TR focal location the vibration amplitude is such that salt may be launched into the air, while the salt remains nearly in contact with the plate at other spatial locations. Additionally, an object placed at the focal location can be knocked over at the time

---

of maximal focusing. These demonstrations are achieved with a single vibration transducer that provides a concentration of energy at a remote location in the plate due to the focusing properties of TR. A scanning laser Doppler vibrometer (SLDV) is used to record the impulse response, needed for TR, at the desired focal location. Other, less-expensive, vibration sensors, such as accelerometers should be possible to use to record the impulse response. The SLDV is also used here to image the concentration of the spatial focusing at the focal location.

One common educational demonstration similar to the one proposed here is the Chladni plate demonstration. In Chladni's demonstration, salt is sprinkled over a plate. The plate is vibrated at a resonance frequency, often using a shaker, though a violin bow may also be used.<sup>13</sup> This causes the salt on the plate to vibrate significantly and accumulate at the nodal lines of the modal pattern for that resonance frequency.<sup>14,15,16</sup> The TR focusing demonstration presented here provides an impulsive focusing of energy at a single location on the plate, rather than continuous wave excitation of a mode that globally vibrates the plate as in Chladni's demonstration.

## II. Experiment Setup

TR has been shown to be successful with a single source transducer.<sup>17</sup> In order for a single channel TR experiment to successfully provide a focus, the impulse response must contain many reflected paths between the source and the receiver. Each reflected path can be exploited to create an image source in the TR process. Thus a long reverberation time (RT60) is desirable. Six different plates, of different materials, are selected, which were readily available, to determine which would provide the best TR focusing. Table 1 provides the information about the plates tested. The materials include cardboard, medium density fiberboard (MDF), particle board, steel,

---

aluminum, and glass. The plates are somewhat similar in size, but this study's scope did not include different sizes of plates of the same material. Larger plates should provide longer reverberation times, until the point at which attenuation of the vibrations dominates, thereby yielding a decreasing reverberation time with increasing plate size. The intent here is to describe a procedure for someone to select the best plate available rather than to specify an optimal plate material and size. A larger aluminum plate, measuring  $183 \times 122 \times 0.32 \text{ cm}^3$  was purchased for nearly \$600 USD, and demonstrations using this plate are described in Section IV, however due to its high cost it is not included in this focusing quantification study.

**TABLE 1. List of the plate materials used in this study, their densities, and their sizes.**

Plate Material	Density (kg/m <sup>3</sup> )	Length (m)	Width (m)	Thickness (mm)
Cardboard	170	0.959	1.092	6.4
MDF	760	0.787	1.201	12.7
Particle board	680	1.219	1.208	11.1
Steel	780	1537	1.092	2.0
Aluminum	2700	0.686	0.813	3.2
Glass	2500	1.016	1.524	2.4

The experiment is setup by placing a plate on top of rubber stoppers for support. A Polytec PSV-400 Scanning Laser Doppler Vibrometer (SLDV) is positioned above the plate and the laser spot is positioned away from the boundaries and the vibration source. A shaker, a mighty dwarf vibration speaker, is placed at a random location on the plate. Figure 1 displays a schematic drawing of the setup and includes a photograph of the glass plate with salt sprinkled on it. The demonstration depicted in Fig. 1 is setup on an optical table, visible through the glass, but the use

of a specialized table is not necessary. The shaker is first used to broadcast a logarithmic chirp signal. This chirp signal sweeps from 500 Hz to 5,000 Hz. At 500 Hz the wavelength in the each plate is approximately one third of the plate's width dimension; higher frequencies create smaller TR focal regions. Above 5,000 Hz the shaker's output efficiency drops off significantly. The source in each experiment that follows is the shaker, whereas the sensor in each experiment that follows is the SLDV.

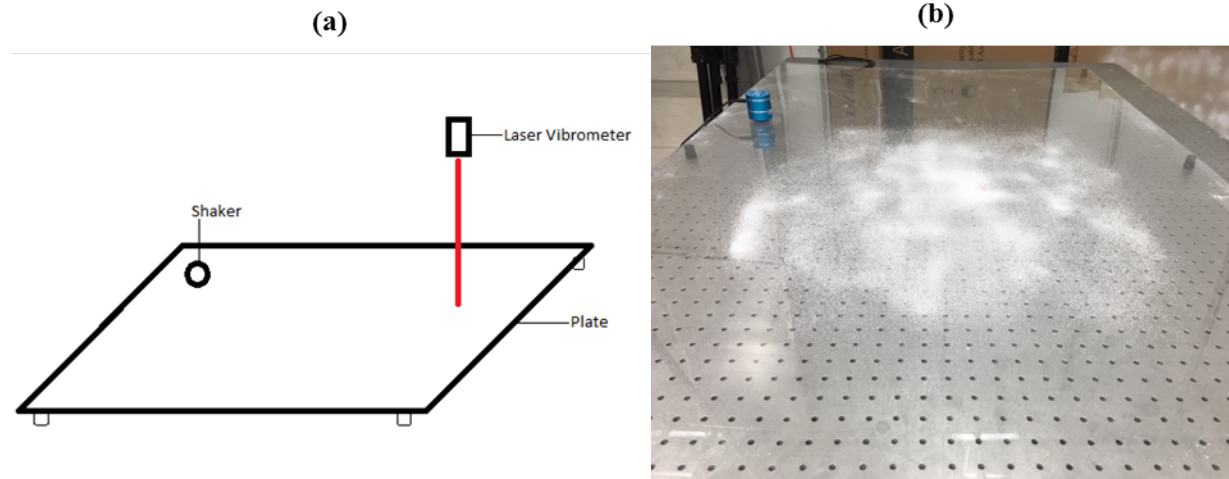


**FIG. 1. (a)** Diagram of the experiment setup. **(b)** Photograph of experiment setup with a glass plate, the shaker in the upper left of the photo, and salt sprinkled onto the plate.

The use of a chirp signal allows one to extract a high quality impulse response. A cross correlation of the chirp signal,  $s(t)$ , that is broadcast from the shaker and the chirp response,  $r(t)$ , measured by the SLDV yields the impulse response

$$ir(t) = \int_T s^*(t) r(t + \tau) d\tau , \quad (1)$$

where  $T$  is the signal length and  $*$  represents a complex conjugate. It should be noted that  $ir(t)$  is a *band-limited* impulse response, or Green's function between the source and the receiver, and

that the amplitude of the impulse response may not have an absolute significance, but that relative differences between impulse response measurements on different plates has meaning. Figure 2 displays sample signals obtained on the glass plate. Note the difference in time scales for Figs. 2(a) and 2(b) compared to Figs. 2(c) and 2(d). A time reversal of  $ir(t)$  is performed and  $ir(-t)$  is then broadcast from the shaker. The TR focus is displayed in Fig. 2(d). Note the peak amplitude of 36.4 mm/s is 3.2 times higher than the highest peak in the chirp response signal (11.5 mm/s), showing the impulsive focusing power of the TR process.

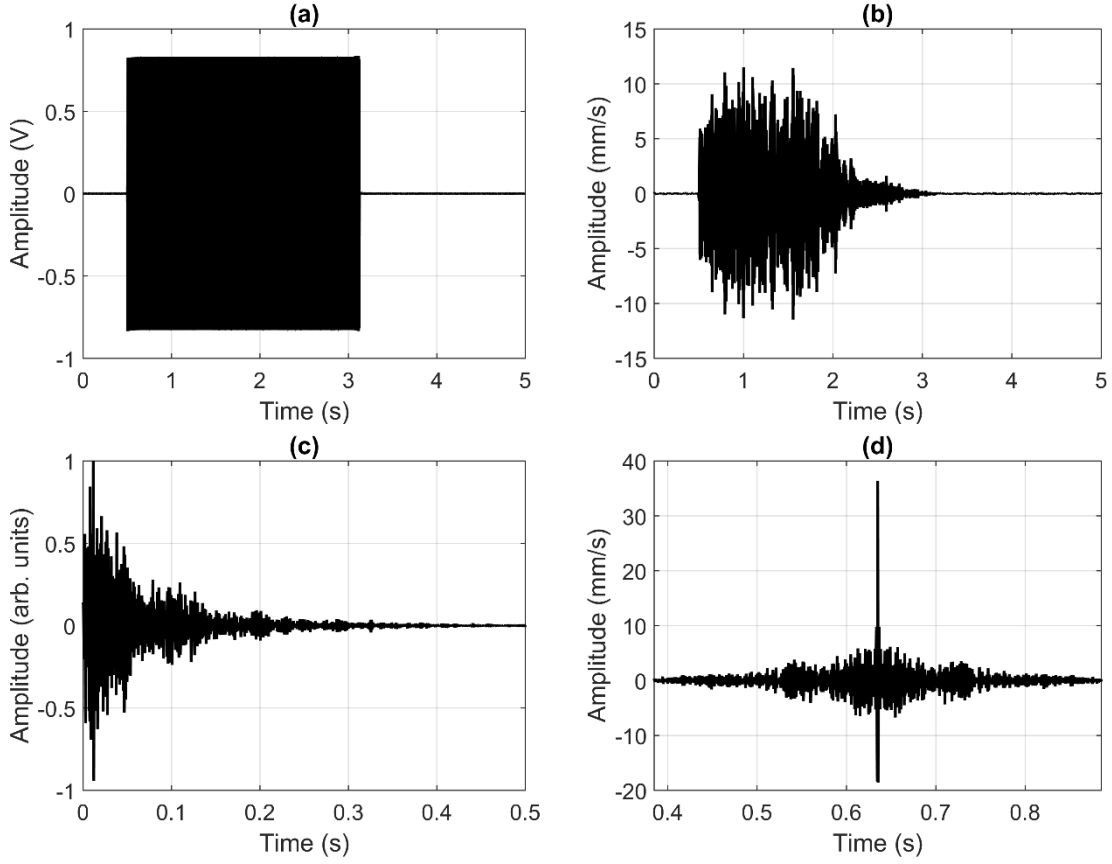


**FIG. 2. Sample signals from a time reversal experiment. (a) Chirp signal sent to the source. (b) Chirp response recorded by the laser vibrometer on the glass plate. (c) Impulse response extracted from the cross correlation. (d) Focal signal recorded by the laser vibrometer when the reversed impulse response is broadcast from the source.**

---

In order to quantify a reverberation time and an output efficiency, a set of impulse responses are determined using the chirp method previously described. The SLDV sensor is placed at three different locations, while the shaker is placed at three different locations. An impulse response is determined for each sensor and source location, producing a total of nine impulse responses. For each measurement, ten time averages are used to increase the signal to noise ratio. Signal triggering is used in order to time sync the averages when the signal reaches 10% of dynamic range. A 10% pre-trigger is also used to ensure that the signal onset is recorded. For these measurements  $T = 5$  s and the dynamic range is set to 10 V. The SLDV sensitivity is set to 5 mm/s/V for the chirp response recording and 125 mm/s/V for the scans of the time reversal focusing.

A reverse Schroeder integration is performed on each impulse response in the set for each plate according to

$$RSI(t) = \int_T^0 ir^2(t)dt \quad (2)$$

where  $RSI$  is the reverse Schroeder integration result.<sup>18</sup> Since the reverberation times in some plates were very short, care was taken to avoid changes in the slope of the integration curve due to the background noise, meaning that it wasn't always possible to extract the decay rate from the -5 dB to -35 dB down points on the curve as specified by the room acoustics standards.<sup>18</sup> The RT60 value was obtained by extrapolating whatever decay amount could be reasonably determined from  $RSI$  to the amount of time it takes for the  $RSI$  to decay 60 dB from an initial value.

A frequency response,  $H(f)$ , may be calculated by taking the Fourier transform of  $ir(t)$ . An integration of  $|H(f)|$  over the input bandwidth of 500-5000 Hz allows quantification of an output efficiency,  $\eta$ , representing the coupling of energy from the shaker into vibrations of the plate over the measurement bandwidth. A peak frequency,  $f_p$ , can also be determined from a

---

smoothed  $|H(f)|$  over the input bandwidth. The wavelength of the peak frequency gives an idea of how large the focal spot's diameter may be.

The  $RT60$ ,  $\eta$ , and  $f_p$  may be used to make a hypothesis about which plate material would yield the peak amplitude TR focus,  $A_p$ , and which plate would yield the highest focal quality in terms of the concentration of the focal energy in time,  $\xi_T$ , and space,  $\xi_S$ .

In order to test the relation of the above mentioned metrics to the TR performance, TR is performed on the plates. In order to quantify  $\xi_S$ , an SLDV must be used. However, since educators attempting to setup this demonstration may not have a SLDV at their disposal, it would be useful to only need to quantify the  $RT60$ ,  $\eta$ , and  $f_p$  from impulse response measurements that can be measured at a single point with a laser vibrometer or a cheaper vibration sensor, such as an accelerometer. Thus a scan of the time reversal focusing on each of the plates is conducted to see how the impulse response metrics correlate with the time reversal performance metrics  $A_p$ ,  $\xi_T$ , and  $\xi_S$ .

For a spatial scan of a TR focusing wave field, the data set would consist of  $N_x$  by  $N_y$  time signals,  $A(x, y, t)$ . The  $A_p$  is the maximum of the absolute value of the temporal focal signal,  $A(x_0, y_0, t)$ , which is measured at the focal position  $(x_0, y_0)$ . The temporal focal quality of a TR experiment is

$$\xi_T = \frac{[A_p]^2}{\frac{1}{N} \int_0^T [A(x_0, y_0, t)]^2 dt}, \quad (3)$$

where the integration of each discrete time step between 0 and  $T$  is included. Thus a delta function signal, representing an ideal-though-impossible TR signal, would have a value  $\xi_T = N$ . A

---

sine wave signal, where the peak amplitude is no larger than other peaks in the signal, would have a value  $\xi_T = 2$  for large  $N$ . As a final example, a flat line of any magnitude would have a value of  $\xi_T = 1$ , because the peak is equal to the average value. At the focal time,  $t_F$ , the data set is reduced to a map in space at  $t_F$ , or  $A(x, y, t_F)$ . The spatial focal quality of a TR experiment is

$$\xi_S = \frac{[A_p]^2}{\frac{1}{N_x N_y} \int_1^{N_x} \int_1^{N_y} [A(x, y, t_F)]^2 dx dy}. \quad (4)$$

The deconvolution technique, or inverse filter, applied to TR has been shown to produce a sharper TR focus, often at the expense of TR focal amplitude.<sup>19,20,21,22</sup> In the context of the goal of this demonstration, a large  $A_p$  is desired but high values of  $\xi_T$  and  $\xi_S$  are desired also. Additionally, the **TR signal that will be broadcast** may be **intentionally clipped in order to increase the focal amplitude**. When the TR signal is clipped the timing of the impulse response is preserved, but the direct signal and early reflections no longer dominate the TR signal, yielding a larger  $C$ . To intentionally clip the TR signal, one can start by normalizing the TR signal and then multiplying it by a desired number,  $C$ . Then every positive TR signal value that exceeds  $C$  is set equal to  $C$ , while every negative TR signal value that is less than  $-C$  is set equal to  $-C$ . For the glass plate various values of  $C$  were used to determine an optimal  $C = 10$  in terms of  $A_p$  while minimizing the corruption of  $\xi_T$  as happens with increasing  $C$ . Figure 3 illustrates the effects of incorporation deconvolution and clipping to  $y_{TF}(t)$ . For the deconvolution signal  $A_p = 29.1$  mm/s compared to  $A_p = 36.4$  mm/s for standard TR (without deconvolution), representing a reduction of 20% in peak amplitude. The shaker has internal amplification, which increases the peak amplitude by a factor of 3.6. When the deconvolution signal is clipped ( $C = 10$ ) and amplified, the  $A_p = 386.8$  mm/s, represents a gain of a factor of 13.3 over the deconvolution  $y_{TF}(t)$

without clipping and amplification. It also represent a gain of 10.6 over the standard  $y_{TF}(t)$  without clipping and amplification. When standard TR is clipped and amplified, the resulting  $\xi_T$  is noticeably lower than when deconvolution TR is clipped and amplified, though the  $A_p$  is slightly higher with standard TR. Clearly more energy (total amplitude over time) is broadcast in the signal displayed in Fig. 3(c) than in Fig. 3(a). The TR focal quality,  $\xi_T$ , is also noticeably decreased in Fig. 3(d) relative to Fig. 3(b), though the peaks of energy away from the main focus are approximately the same in relation to the main focal peak for the signals in both figures.

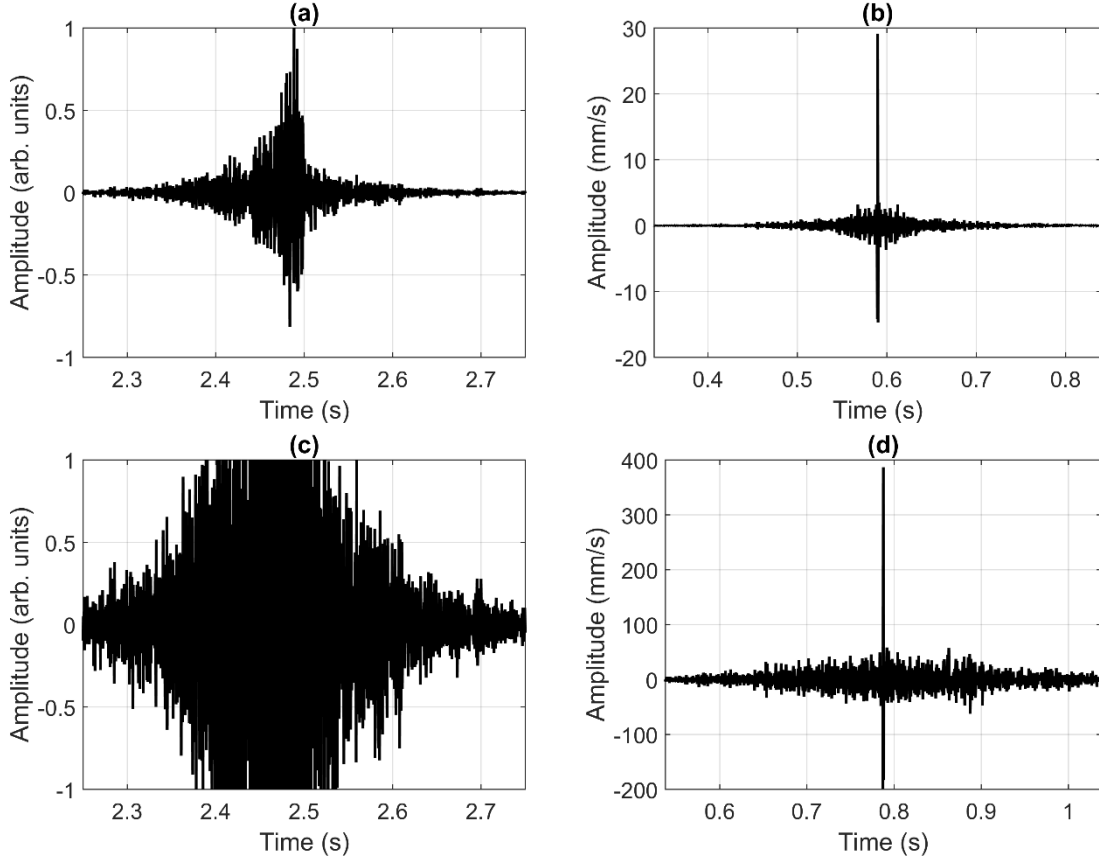


**FIG. 3. Deconvolution time reversal (TR) signals obtained on the glass plate. (a) Deconvolution TR signal without clipping. (b) Deconvolution TR focal signal without clipping. (c) Deconvolution TR signal with 10 times clipping. (d) Deconvolution TR focal signal with 10 times clipping.**

---

The TR focusing occurs at the location where the chirp response is recorded. Scans of the velocity wave fields during TR focusing are done with the SLDV. The same settings of the laser vibrometer with regards to sensitivity, triggering, and maximum response were used in this part of the experiment as used previously. For the scans of TR focusing in each plate, the deconvolution technique, signal clipping (times 10), and amplification are used.

### III. Results

The scans of the TR focusing wave fields on each plate are done with a 27 by 37 point scan grid, where the spacing between each scan point is 2.0 cm. As previously stated, a deconvolution is applied to the impulse response signal. The deconvolution signal is then intentionally clipped by a factor of 10 and amplified by the shaker's internal amplifier. Three time averages are used for each scan point. Developer spray was applied to each plate surface to enhance the reflectivity of the laser light. Figure 4 displays the spatial distribution of the TR focusing at the time of peak focusing (the value at each point in space is squared to represent a map of the instantaneous energy). Somewhat surprisingly, a decent level of TR focusing was achieved in each plate material, including in the cardboard and wooden plates. Figure 4 illustrates the vast improvement of the spatial confinement of the focusing in the glass plate as compared to that in the cardboard plate and also the much higher  $A_p$  in the glass than in the cardboard.

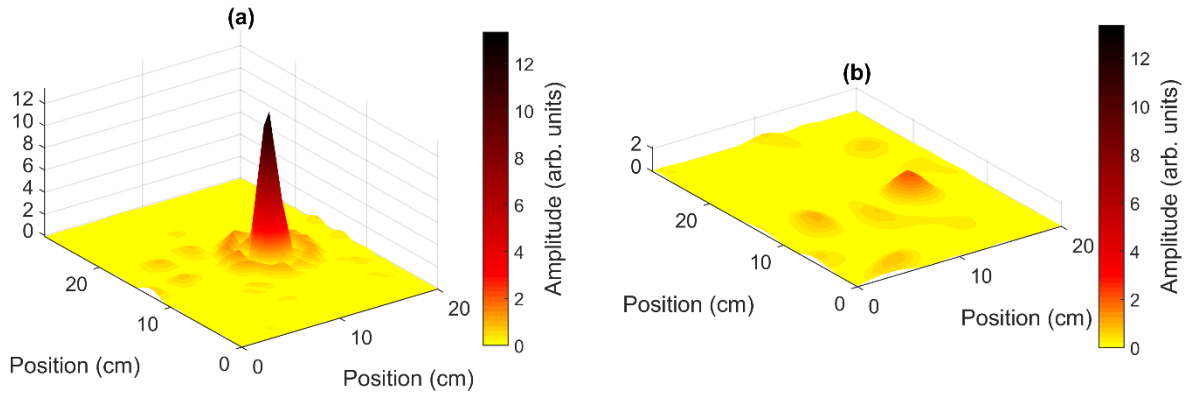


**FIG. 4. Spatial maps of the instantaneous energy at the time of peak time reversal focusing. (a) Glass plate. (b) Cardboard plate. Color denotes amplitude. The peak heights are to scale with respect to each other (meaning 2 units on the z-axis is the same for both plots).**

The impulse response metrics of  $RT60$ ,  $\eta$ , and  $f_p$  are given in Table 2. These values represent average values computed from each of the nine impulse response signals in the set for each plate. The TR focal signal quality metrics of  $A_p$ ,  $\xi_T$ , and  $\xi_S$  are also given in Table 2. The best TR focusing occurs in the glass plate and the worst TR focusing occurs in the cardboard plate. Even though the cardboard plate yielded a slightly higher  $\eta$  value than the glass plate did, the time reversal focal amplitude,  $A_p$ , is 2.6 times higher in the glass plate than in the cardboard plate. Thus the output efficiency  $\eta$  value is not a good indicator of the amplitude of the TR focusing by itself. The plates listed in Table 2 are approximately listed in order of increasing  $RT60$ . When comparing the  $\xi_T$  and  $\xi_S$  metrics, the glass plate outperformed the cardboard plate by a factor of 2.8 and 5.1, respectively and the glass plate's metrics were highest among all plates. It appears that the TR focusing quality, whether in space or time, is correlated with the  $RT60$ . The correlation of TR focusing quality and  $RT60$  is to be expected since more reflections used in the TR process provide more virtual sources that contribute to the TR focusing. The steel and alumi-

---

num plates also had high  $RT60$  values, in fact values higher than in glass, but they yielded lower TR focusing quality values. Thus the combination of high  $\eta$  and  $RT60$  values yields both a large amplitude focus and a spatially constrained focus.

**TABLE 2. Table of  $RT60$ ,  $\eta$ ,  $f_P$ ,  $A_P$ ,  $\xi_T$ , and  $\xi_S$ .**

	$RT60$ (s)	$\eta$ (arb. units)	$f_P$ (Hz)	$A_P$ (m/s)	$\xi_T$	$\xi_S$
Cardboard	0.13	29.0	510	0.135	213	13.3
MDF	0.16	3.79	770	0.037	246	18.3
Particle Board	0.18	4.73	880	0.043	329	23.8
Steel	0.79	1.00	1022	0.158	322	60.5
Aluminum	0.85	16.7	990	0.273	204	30.9
Glass	0.78	27.7	1090	0.365	602	68.2

## IV. Demonstration

The evolution of TR focusing from the SLDV can be visualized using Polytec's PSV software. Figure 5 shows five frames that display the evolution of the focusing in space along with the temporal signal recorded at the focal location. The dashed lines indicate the instants in time for the spatial images on the left. The positive phase circular wave fronts visible in the upper two spatial images are traveling inward toward the focal location. The positive phase circular wave fronts visible in the lower two spatial images are traveling outward away from the focal location.

Polytec's software provides a movie of the wave propagation that clearly shows the converging waves that constructively interfere at the focal location and then diverge away. This section describes some ways to visualize the impulsive focusing power of TR.

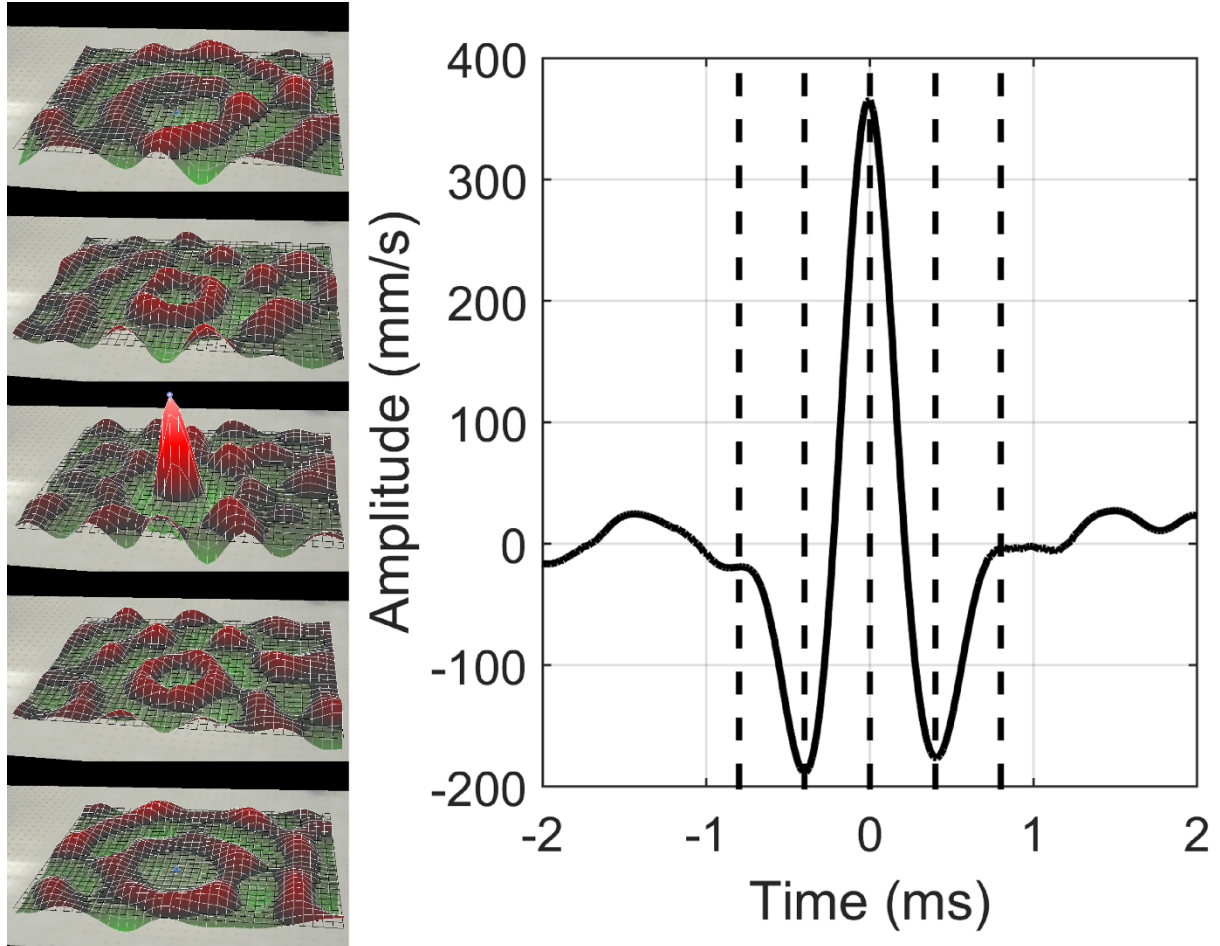


**FIG. 5. Evolution of the time reversal focusing over time. Spatial maps at different time intervals (left) and focal signal at focal location (right). Dashed lines indicate times corresponding to the spatial maps.**

A visualization of the focusing may be done by sprinkling salt on the plate after the chirp response signal has been recorded. When the waves coalesce at the focus location and constructively interfere, the plate vibrates significantly at that location. Figure 6 shows a photograph, tak-

---

en with a high speed camera (iPhone 6S at 200 frames/s), at the instant in time,  $T_f$ , corresponding to when the salt begins to be thrown off of the plate surface. Also shown in Fig. 6 is a few frames after  $T_f$ . The salt is thrust upward 2 cm above the plate. Considering the salt as undergoing projectile motion, the initial velocity,  $v_0$ , of the salt should equal  $v_0 = \frac{1}{2}gt$ , where  $g = 9.8 \frac{\text{m}}{\text{s}^2}$  is the acceleration due to gravity, and  $t$  is the time in which the salt is thrown upward until it returns to the plate. If we assume that  $t = 80\text{ms}$ , then  $v_0 = 392 \frac{\text{mm}}{\text{s}}$ , which is close to the peak velocity measured by the laser vibrometer  $A_p = 365 \frac{\text{mm}}{\text{s}}$ . If a time derivative of the velocity signal in Fig. 5 is applied, then the peak positive acceleration is  $2420 \frac{\text{m}}{\text{s}^2}$  (247 times the acceleration due to gravity), which occurs at approximately  $-0.5\text{ms}$  in Fig. 5.

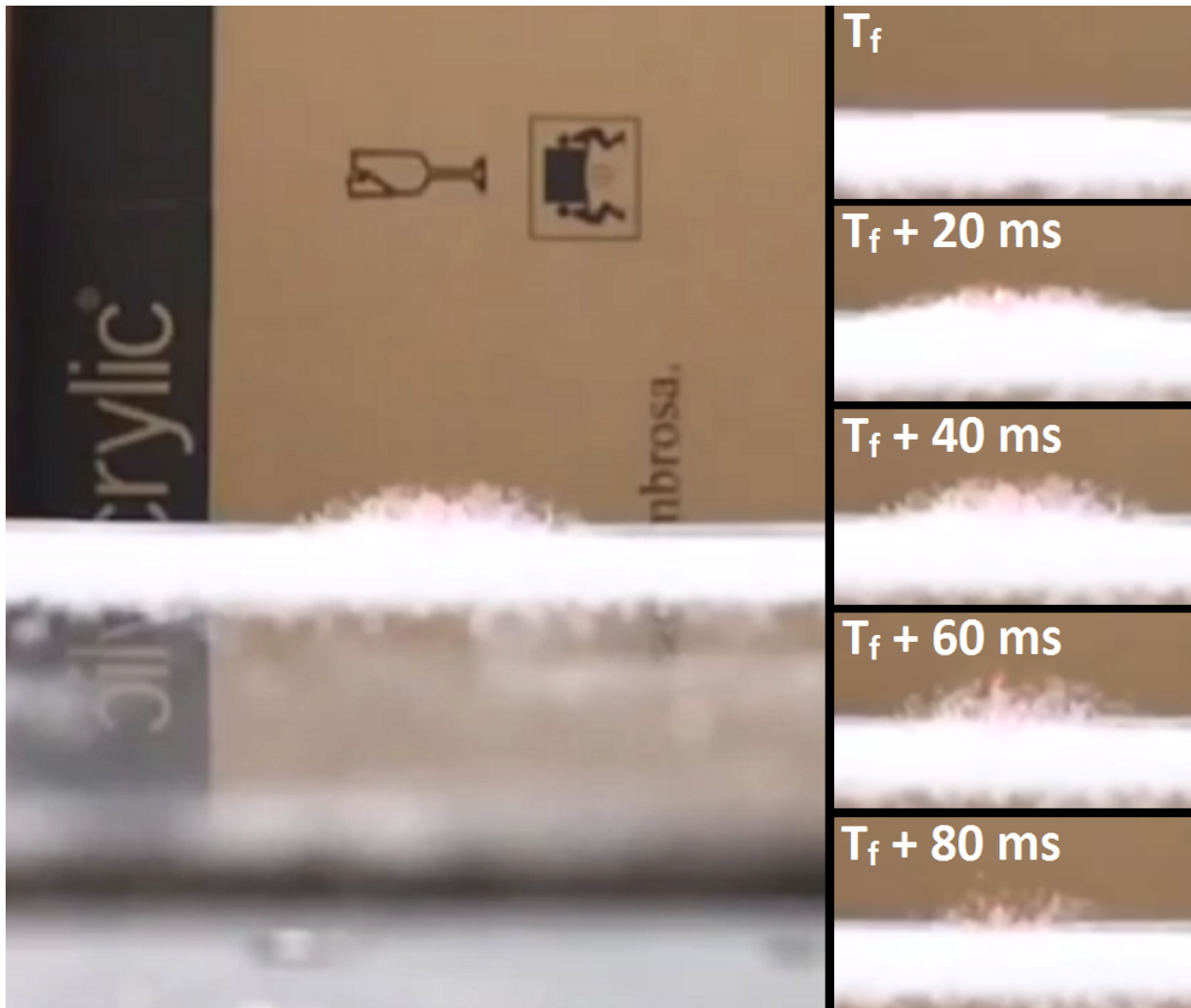


**FIG. 6. Photograph of salt jump visualization at the time of focus  $T_f$  (left) and snapshots before, during, and after the focus (right).**

Another demonstration that works fairly well, though not always repeatable, is to setup an object that is stiff and lightweight at the focal position so that it may be thrust into the air and knocked over. Figure 7 displays images of a few different items being knocked over when they are placed at the focal position for the glass plate and on a larger aluminum plate than studied previously in this paper. The larger aluminum plate measures  $183 \times 122 \times 0.32 \text{ cm}^3$  and is not included in the preliminary study since its cost was nearly \$600.00 USD, which is deemed too

---

expensive to recommend for this demonstration, whereas the aluminum plate studied earlier is a scrap piece of aluminum. We have found that small wooden corks, small cardboard cylinders, and lighter weight cable adapters can be knocked over at the focal position repeatedly while not being knocked over anywhere else on the plate at least 10 cm from the focal position. Lego minifigures are appealing for this demonstration to get the attention of children, but the minifigures are somewhat unstable and while the Lego minifigure setup at the focal position is the most likely to be knocked over, sometimes it does not get knocked over. Additionally, the Lego minifigures setup at locations away from the focal position sometimes get knocked over, though less frequently. In each of the photos depicted in Fig. 7, the inset image shows the undisturbed state of the object prior to the focusing while the background image is of the object being thrown into the air as it's being knocked over. In the case of the Lego minifigures, all of the figures move during the focusing but only the figure in the middle of the photo is knocked off of his feet. In the case of Figs. 7(a) and 7(b), the focusing can be repeated successively as the object (cardboard cylinder and cable adapter) is placed at different locations on the plate. Even if the object is placed near the source the vibrations are not large enough to knock over the object unless it is placed at the focal location.

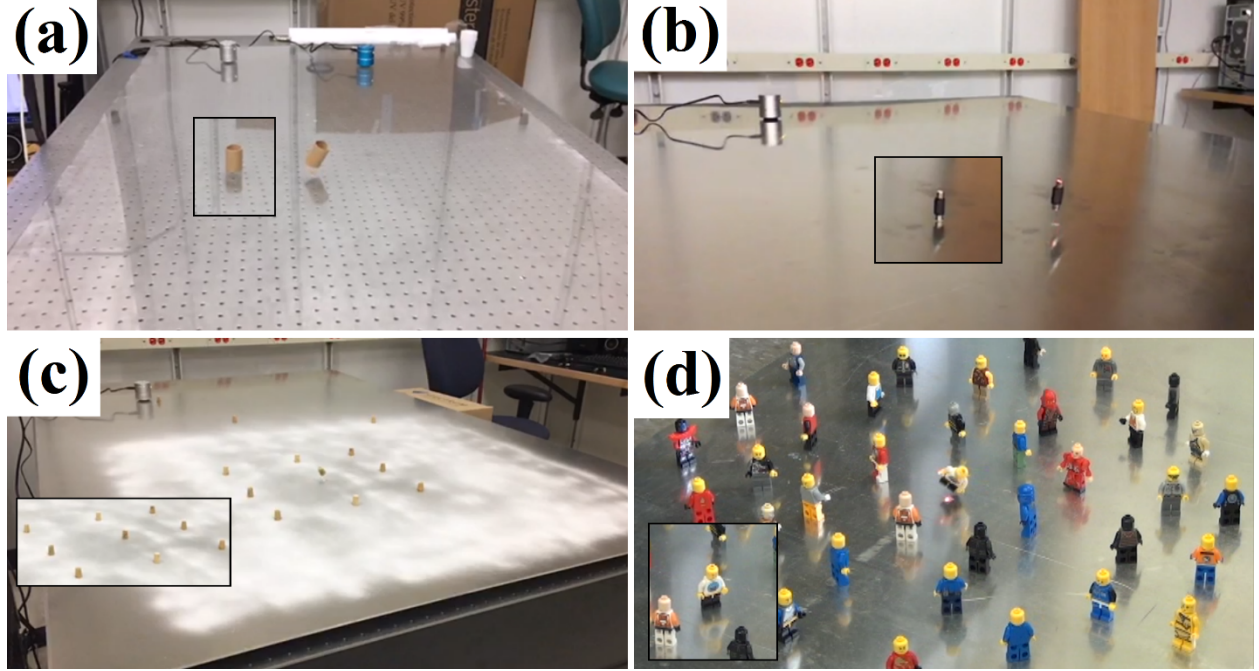


**FIG. 7. Photographs of time reversal focusing being used to knock over objects. The inset image, outlined in black, shows the undisturbed state. (a) a cardboard cylinder is knocked over on the glass plate. (b) an RCA adapter, (c) a wooden cork (developer spray was applied to allow laser scanning), and (d) a Lego minifigure are knocked over on the large aluminum plate.**

An important consideration that remains to be addressed in order to keep this demonstration from being overly expensive is the vibration sensor. The demonstrations shown here have employed a laser Doppler vibrometer (LDV), which cost tens of thousands of U.S. dollars at minimum (lasers with scanning capabilities are in the hundreds of thousands of dollars range). The LDV directly senses velocity as a function of time. Thus if a position or acceleration versus time sensor is used, then the higher frequencies will be under represented or over represented, respectively, relative to lower frequencies in comparison to velocity sensors. We recommend the use of inexpensive accelerometers as a cheap vibration sensing option. The dominant frequencies used in these demonstrations were in the neighborhood of 1000 Hz, so frequency bandwidth and the sensitivity of the sensor should be considered.

---

## IV. Conclusion

This paper has described a demonstration of spatially-confined, time reversal focusing of vibrations in thin plates using a single source transducer and a single receiver. The focusing performance metrics (peak amplitude, spatial quality, and temporal quality) indicate that the  $1.016 \times 1.524 \times 2.4 \text{ mm}^3$  glass plate was the best plate for a demonstration. Metrics that quantify properties of the impulse response in a plate were described. It was found that the combination of high reverberation time and sensitivity metrics was found to be a good indicator of spatially localized focusing and large amplitude focusing. Some plates had high reverberation times but low efficiencies (aluminum and steel plates), while the cardboard plate had a high efficiency but a low reverberation time, and in each of these cases the focusing performance was weaker than in the glass plate. The glass plate had a reverberation time of 0.78 seconds and its efficiency was comparable to cardboard and nearly twice the efficiency of the aluminum plate. In addition, glass is significantly less expensive and more accessible than aluminum, which gave the next best focusing performance.

A deconvolution operation was employed to provide a sharp focusing in time. Focusing amplitude was found to be enhanced by a factor of 13.3 when the time reversed deconvolution signal was intentionally clipped by a factor of 10 prior to amplifying and broadcasting the signal to create the focusing. A peak velocity of 365 mm/s was achieved in the glass plate along with a peak acceleration of 247 times the acceleration due to gravity.

Salt was sprinkled onto the glass plate and the focusing demonstration was used to make the salt visibly jump off of the plate only at the selected focusing location. Additionally, demonstrations of the ability of time reversal to knock over objects were shown, including knocking over cardboard cylinders, cable adapters, wooden corks, and Lego minifigures. The salt jumping

---

demonstration may be the best live demonstration since the observer can clearly see the localized nature of the high amplitude focusing of elastic waves in a plate. The Lego minifigures were not knocked over consistently enough to provide a reliable demonstration due to their inherent instabilities.

Further research should explore the effect of the plate thickness and plate size of the focusing performance since it is expected that the reverberation time, for larger plates in particular, will vary with the dimensions of the plate. Additionally this research did not focus on the use of an inexpensive vibration sensor and further work could compare the use an accelerometer to a laser Doppler vibrometer. Finally, one might easily employ two source transducers from their computer's stereo outputs to produce a larger and more spatially confined focus of energy.

---

## Bibliography

- <sup>1</sup> M. Fink, "Time reversed acoustics," *Phys. Today* **50**(3), 34-40 (1997).
- <sup>2</sup> B.E. Anderson, M. Griffa, C. Larmat, T.J. Ulrich, and P.A. Johnson, "Time reversal," *Acoustics Today* **4**(1), 5-16 (2008).
- <sup>3</sup> A. Parvulescu and C. Clay, "Reproducibility of signal transmission in the ocean," *Radio Electron Eng.* **29**(4), 223-228 (1965).
- <sup>4</sup> C. He, Q. Zhang, and J. Huang, "Passive time reversal communication with cyclic shift keying over underwater acoustic channels," *Applied Acoustics* **96**(9) 132-138 (2015).
- <sup>5</sup> G. Zhang, J.M. Hovem, D. Hefeng, and L. Liu, "Coherent underwater communication using passive time reversal over multipath channels," *Applied Acoustics* **72**(7), 412-419 (2011).
- <sup>6</sup> B.E. Anderson, M. Griffa, T.J. Ulrich, P.-Y. Le Bas, R.A. Guyer, and P.A. Johnson, "Crack localization and characterization in solid media using time reversal techniques," *44<sup>th</sup> US Rock Mechanics Symposium and 5<sup>th</sup> U.S.-Canada Rock Mechanics Symposium*, (June 2010, Salt Lake City, UT).
- <sup>7</sup> P.Y. Le Bas, M.C. Remillieuz, L. Pieczonka, J.A. Ten Cate, B.E. Anderson, and T.J. Ulrich, "Damage imaging in a laminated composite plate using an air-coupled time reversal mirror," *Appl. Phys. Lett.* **107**(18), 184102 (2015).
- <sup>8</sup> B.E. Anderson, T.J. Ulrich, P.-Y. Le Bas, and J.A. Ten Cate, "Three dimensional time reversal communications in elastic media," *J. Acoust. Soc. Am.* **139**(2), EL25-EL30 (2016).
- <sup>9</sup> C.S. Larmat, R.A. Guyer, and P.A. Johnson, "Time-reversal methods in geophysics," *Physics Today* **63**(8), 31-35 (2010).
- <sup>10</sup> C.S. Larmat, R.A. Guyer, and PA. Johnson, "Tremor source location using time-reversal: selecting appropriate imaging field," *Geophys. Res. Lett.* **36**(22), L22304 (2009).
- <sup>11</sup> M. Fink, "Time-reversal acoustics in biomedical engineering," *Annual Review of Biomedical Engineering* **5**(1), 465-497 (2003).
- <sup>12</sup> M. Fink, "Time reversal and phase conjugation with acoustic waves: industrial and medical applications," *Lasers and Electro-Optics* **3**, 2334-2335 (2005).

- 
- <sup>13</sup> T. Neilsen, W. J. Strong, K. L. Gee, B. E. Anderson, S. D. Sommerfeldt, and T. W. Leishman, “Creating an active-learning environment in an introductory acoustics course,” *J. Acoust. Soc. Am.* **131**(3), 2500-2509 (2012).
- <sup>14</sup> F. Lemoult, M. Fink, and G. Lerosey, “Acoustic resonators for far-field control of sound on a subwavelength scale,” *Physical Review Letters* **107**(6), 1-6 (2001).
- <sup>15</sup> H.J. van Gerner, K. van der Weele, M.A. van der Hoef, and D. van der Meer, “Air-induced inverse Chladni patterns,” *Journal of Fluid Mechanics* **689**, 203-220 (2011).
- <sup>16</sup> T.D. Rossing, “Chladni’s law for vibrating plates,” *American Journal of Physics* **50**, 271-274 (2010).
- <sup>17</sup> A.M. Sutin, J.A. Ten Cate, and P.A. Johnson, “Single-channel time reversal in elastic solids,” *J. Acoust. Soc. Am.* **116**(5) 2779-2784 (2004).
- <sup>18</sup> ISO 3382:1997(E). “Acoustics – Measurement of the reverberation time of rooms with reference to other acoustical parameters.” (International Organization for Standardization, Geneva, Switzerland, 1997).
- <sup>19</sup> M. Tanter, J.-L. Thomas, M. Fink, “Time reversal and the inverse filter,” *J. Acoust. Soc. Am.* **108**, 223-234 (2000).
- <sup>20</sup> M. Tanter, J.F. Aubry, J. Gerber, J.-L. Thomas, M. Fink, “Optimal focusing by spatio-temporal filter. I. basic principles,” *J. Acoust. Soc. Am.* **110**, 37-47 (2001).
- <sup>21</sup> T. Gallot, S. Catheline, P. Roux, M. Campillo, A passive inverse filter for Green’s function retrieval, *J. Acoust. Soc. Am.* **131**, EL21-EL27 (2011).
- <sup>22</sup> B. E. Anderson, J. Douma, T. J. Ulrich, and R. Snieder, “Improving spatio-temporal focusing and source reconstruction through deconvolution,” *Wave Motion* **52**, 151-159 (2015).